RSC Advances

PAPER

View Article Online
View Journal | View Issue

Cite this: *RSC Adv.*, 2025, **15**, 15293

An electrospinning deposited cobalt oxide nanofiber gas sensing device: selective enhancement as a thermal electronic nose†

Dang Thi Thanh Le,[ab] Vu Anh Tuan,[ab] Matteo Tonezzer,*[cd] Chu Manh Hung[ab] and Nguyen Duc Hoa*[ab]

Received 6th February 2025
Accepted 30th April 2025

DOI: 10.1039/d5ra00873e

rsc.li/rsc-advances

Cobalt oxide nanofibers (Co_3O_4 NFs) were synthesized using a two-step procedure involving electrospinning followed by calcination. The microstructural, morphological, and elemental properties of the nanofibers were characterized using X-ray diffraction (XRD), transmission electron microscopy (TEM), scanning electron microscopy (SEM), and energy-dispersive spectrometry (EDS). The Co_3O_4 NFs exhibited high structural integrity, chemical purity, and uniform diameters ranging from 20 to 50 nm. Thermal treatment at 600 °C for 3 hours transformed the electrospun fibers into elongated nanofibers composed of interconnected Co_3O_4 nanoparticles. The gas sensing properties of the Co_3O_4 NFs were evaluated for ethanol (C_2H_5OH) detection over a temperature range of 250 to 450 °C. The sensor demonstrated a significant response to ethanol, highlighting their potential for gas sensing applications. When employed as a thermal electronic nose, the device achieved perfect classification (100% accuracy) for six tested gases and demonstrated effective concentration estimation, with an average error of 28.6%.

1. Introduction

Gas sensors have attracted significant attention due to their wide-ranging applications in industrial emissions control, residential safety, environmental monitoring, and medical diagnostics. Among them, metal oxide-based chemoresistor gas sensors, such as those using indium oxide (In_2O_3),[1] tungsten oxide (WO_3),[2] and cobalt oxide (Co_3O_4),[3] have seen substantial advancements. These sensors are valued for their compact size, low production costs, portability, reliability, long lifespan, and ease of use.

Spinel cobalt oxide (Co_3O_4) is a mixed-valence compound comprising CoO and Co_2O_3 phases, exhibiting p-type semiconducting behavior with high oxygen content. It has been extensively studied for various applications, including energy storage,[4] catalysis,[5] sensor technology,[6] and electrochemical systems.[7] Co_3O_4 exhibits outstanding catalytic performance, characterized by high activity, durability, and stability across a range of environmentally relevant applications. Additionally, Co_3O_4 features diverse morphological structures, a high concentration of surface oxygen species, and excellent structural stability, rendering it a highly effective material for gas sensing applications. The gas sensing capabilities of Co_3O_4 are well-documented, with its sensing mechanism primarily relying on surface catalytic interactions. Recent studies reported that Co_3O_4-based gas sensors typically require high operational temperatures, exceeding 200 °C, to achieve optimal performance due to improved catalytic properties and high oxygen content.[8–11] Thus in this study, we tested the sensors in the temperature range from 250 to 450 °C.

Ethanol, a volatile and flammable compound, has a lower and upper explosion limit of 3.3% and 19% in air, respectively, posing risks in industrial and domestic environments.[12,13] Prolonged exposure to ethanol vapor can lead to intoxication, neurological damage, and other health issues. As a result, there is a growing need for advanced ethanol gas sensor for industrial safety and everyday applications.

One-dimensional (1D) nanostructures offer significant advantages for gas sensing properties due to their ability to confine charge carriers transport along a single axis, enhancing charge mobility and sensitivity. Additionally, hollow nanostructures adsorption and desorption kinetics, reducing response and recovery times. For instance, Y. Zhang *et al.* demonstrated that electrospun $LaFeO_3$ nanotubes exhibited enhanced ethanol sensing performance with faster response and recovery times.[14]

Various methods, including thermal evaporation, self-catalytic growth, hydrothermal synthesis, and electrospinning, have been employed to produce 1D nanomaterials.[15] Among these,

[a]*Faculty of Electronic Materials and Devices, School of Materials Science and Engineering (SMSE), Hanoi University of Science and Technology (HUST), No. 1, Dai Co Viet Str., Hanoi, 100000, Vietnam*

[b]*International Training Institute for Materials Science (ITIMS), Hanoi University of Science and Technology (HUST), No. 1, Dai Co Viet Str., Hanoi, 100000, Vietnam. E-mail: ndhoa@itims.edu.vn*

[c]*Department of Chemical and Geological Sciences, University of Cagliari, Campus of Monserrato (CA), Monserrato, I09042, Italy. E-mail: matteo.tonezzer@unica.it*

[d]*Center Agriculture Food Environment, University of Trento/Fondazione Edmund Mach, Via E. Mach 1, San Michele all'Adige, 38010, Italy*

† Electronic supplementary information (ESI) available. See DOI: https://doi.org/10.1039/d5ra00873e

electrospinning particularly attractive due to its simplicity and ability to grow nanomaterials with high length-to-diameter ratios, promoting efficient electron transport.[16]

In this study, Co_3O_4 nanofibers (NFs) were synthesized *via* electrospinning and characterized using scanning electron microscopy (SEM), X-ray diffraction (XRD), transmission electron microscopy (TEM), and energy-dispersive X-ray spectroscopy (EDS). The gas-sensing performance of the Co_3O_4 NFs was evaluated for ethanol detection, demonstrating a strong response, indicating their potential for gas sensing applications. The importance of this work is supported by its ability to accurately discriminate and quantify different gases using a single Co_3O_4 nanofiber sensor in a thermal electronic nose system. This functionality, combined with the relative simplicity of the electrospinning fabrication process, makes these Co_3O_4 nanofibers promising candidates for the development of high-performance ethanol sensors and compact electronic noses with reliable classification and quantification capabilities for a wide range of gases.

2. Materials and methods

2.1. Materials

Cobalt nitrate hexahydrate ($Co(NO)_2 \cdot 6H_2O$, ≥98%) and polyvinyl alcohol (PVA, M_w = 89 000, 99+%) were procured from Sigma-Aldrich and used as received without further purification.

2.2. Sample preparation and characterization

The Co_3O_4 nanofibers were synthesized using a multi-step process, as depicted in Fig. 1. Initially, 1.5 g of polyvinyl alcohol was dissolved in 6 ml of deionized water (DI H_2O) at 130 °C to prepare a white solution (solution A), which was then stirred for 4 hours. Subsequently, 0.5 g of cobalt nitrate hexahydrate ($Co(NO_3)_2 \cdot 6H_2O$) was added to solution A. The resulting mixture (solution B), exhibiting a pink-purple color, was stirred for an additional 14 hours at 60 °C. Solution B was then loaded into a syringe which is at a distance of 13.5 cm to the collector and electrospun for 20 minutes onto silicon substrates with interdigitated platinum electrodes, which were placed on the collector. The pumping speed and the voltage were applied at 0.3 μl h^{-1} and 20 kV, respectively. The deposited nanofibers were dried at 60 °C for 3 hours and subsequently annealed at 600 °C for 3 hours, with a temperature ramp rate of 0.5 °C min^{-1}. This annealing step aimed to enhance the stability of the nanofibers and ensure strong adhesion between the material and the electrodes, resulting in pure Co_3O_4 nanofibers.

The synthesized nanofibers underwent detailed morphological, structural and compositional characterizations. X-ray diffraction (XRD) analysis was performed using a Bruker D5005 diffractometer equipped with CuKα1 radiation (λ = 1.5406 Å), operating at 40 kV and 40 mA, to confirm the crystal structure. High-resolution scanning electron microscopy (SEM) and transmission electron microscopy (TEM) was respectively conducted using a Hitachi-S4800 and a JEOL 2100 microscope at voltage of 5 kV and 200 kV to analyze surface morphology, while elemental composition was determined *via* energy-dispersive spectroscopy (EDS) on the SEM instrument. Thermal properties were evaluated using thermogravimetric analysis (TGA) differential thermal analysis (DTA) with a Linseis TGA 1000 thermal analyzer. The measurements were conducted under ambient air conditions over a temperature range of 26–950 °C, with a heating rate of 2 °C min^{-1}, to assess the material's thermal stability and decomposition behavior.

2.3. Sensor performance evaluation

The gas-sensing performance of the Co_3O_4 nanofiber sensor was evaluated by continuously monitoring its electrical resistance

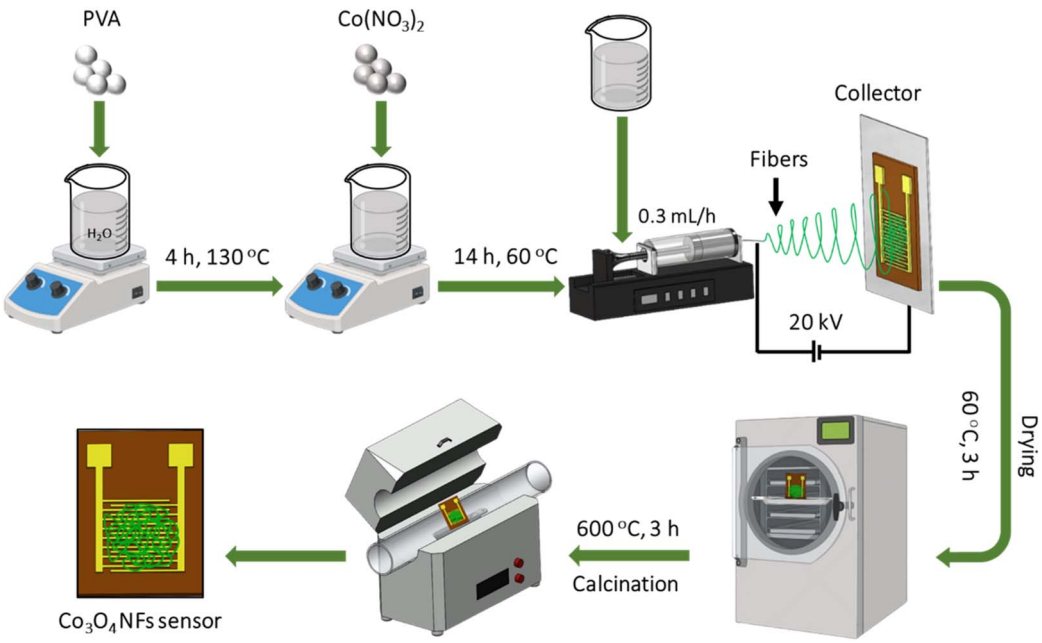

Fig. 1 Synthesis process of Co_3O_4 nanofibers sensor.

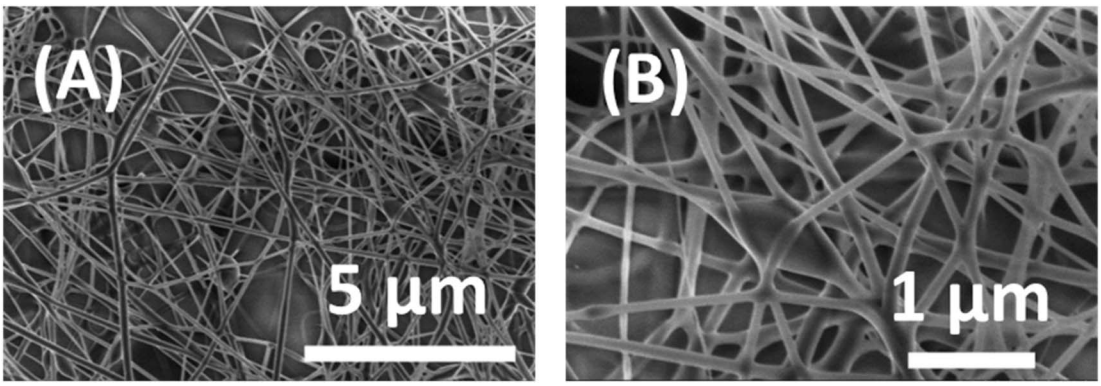

Fig. 2 FESEM images of as-prepared $Co(NO_3)_2$/PVA composite nanofibers: (A) low magnification and (B) high magnification.

using a Keithley 2602 source meter (Keithley, Solon, OH, USA). Three sensors were fabricated and tested for reproducibility. Their response to 500 ppm of ammonia at 350 °C gave a value of 1.68 ± 0.12, demonstrating a good reproducibility (Fig. S1†). The sensor was exposed cyclically to ethanol (C_2H_5OH) gas diluted in air at concentrations ranging from 25 to 500 ppm, ethanol concentrations were precisely controlled using mass flow controllers (MKS, model GV50A), while maintaining a total gas flow rate of 400 standard cubic centimeters per minute (sccm).[17] Sensing experiments were conducted at operating temperatures of 250, 300, 350, 400, and 450 °C in a custom-designed measurement chamber. As cobalt oxide is a p-type metal oxide, the sensor resistance increased upon exposure to ethanol, a reducing gas. The sensor response (S) was calculated as the ratio of the resistance in the presence of ethanol (R_g) to the baseline resistance in air (R_a), expressed as $S = R_g/R_a$. In all calculations, an error of 3 standard deviations was used, corresponding to a significance level of 99.7%.

3. Results and discussion

3.1. Nanofiber characterizations

The morphology of the synthesized Co_3O_4 nanostructures was studied by scanning electron microscopy (SEM). The SEM images of $Co(NO_3)_2$/PVA composite nanofibers, as depicted in Fig. 2, reveal a nonwoven, spiderweb-like structure with randomly oriented fibers. These nanofibers exhibited smooth surfaces and uniform diameters, which were homogeneously distributed, with an average range of 100–300 nm.

The morphological changes induced by annealing were analyzed through SEM imaging, as shown in Fig. 3. After annealing at 600 °C, the Co_3O_4 nanofibers maintained their spiderweb arrangement, with lengths extending to several tens of microns (Fig. 3A). The average diameter, however, decreased to approximately 100–200 nm, attributed to the thermal decomposition of polyvinyl alcohol and the transformation of precursor fibers into crystalline Co_3O_4 nanofibers.

The calcination process was further examined using differential thermal analysis (DTA) and thermal gravimetric analysis (TGA), with results presented in Fig. 4. The TGA curve revealed distinct weight loss stages:

• Initial stage (up to 220 °C): a weight loss of ∼30%, attributed to the evaporation of low boiling points components, such as residual water.[18]

• Intermediate stage (220–340 °C): a slower weight loss (∼18%), associated with the decomposition of $Co(NO_3)_2$ and intermolecular cross-linking reactions.[19–21] Concurrently, the degradation of PVA's side chains and the loss of –OH groups resulted in the formation of conjugated and non-conjugated polyenes.[15–17]

• Final stage (350–470 °C): a substantial weight loss (∼40%), with an endothermic peak at 370 °C, due to carbon oxidation and the complete decomposition of residual PVA structures.[22]

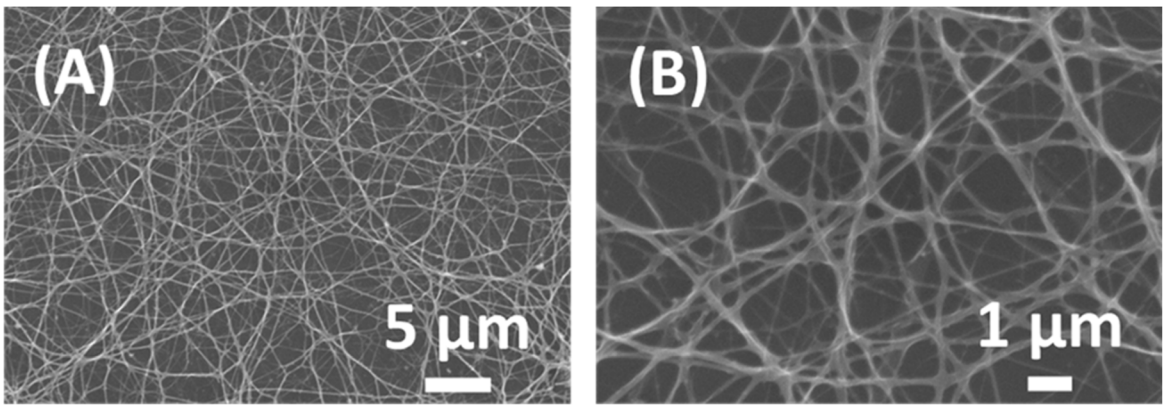

Fig. 3 SEM images of annealed Co_3O_4 nanofibers: (A) low magnification and (B) high magnification.

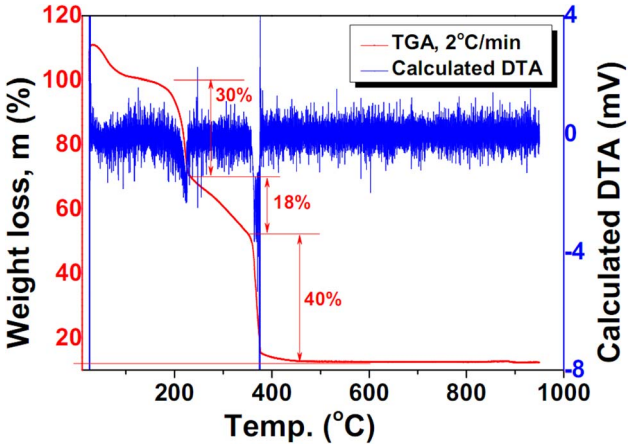

Fig. 4 DTA-TGA curves of the $Co(NO_3)_2$/PVA composite nanofibers.

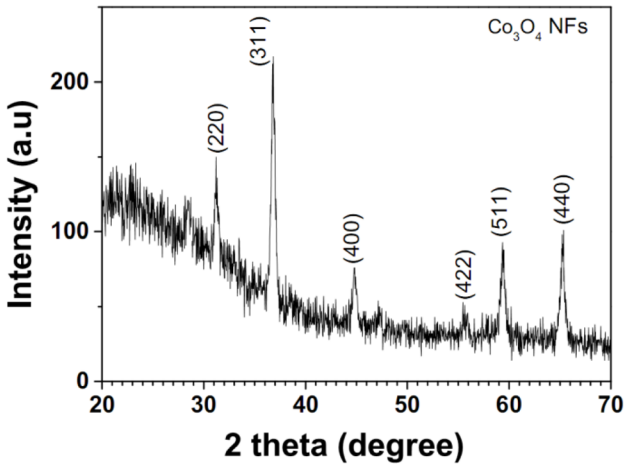

Fig. 6 XRD pattern of the annealed Co_3O_4 NFs.

The elemental composition of the annealed nanofibers was examined using energy dispersive spectroscopy (EDS) and elemental mapping, as illustrated in Fig. 5. The EDS elemental spectrum confirmed the presence of cobalt (Co) and oxygen (O), with silicon (Si) originating from the Si/SiO_2 substrate (Fig. 5B). Elemental mapping further demonstrated the homogeneous distribution of Co and O within the nanofibers (Fig. 5C–E).

X-ray diffraction analysis (Fig. 6) identified six distinct peaks corresponding to the cubic spinel phase of Co_3O_4, indexed to crystalline planes (220), (311), (400), (422), (511), and (440) (JCPDS 042-1467).[23] The absence of peaks related to impurities or amorphous phases confirmed the high crystallinity of the synthesized material.

Transmission electron microscopy provided further insights into the microstructure of the Co_3O_4 nanofibers (Fig. 7). Low-magnification TEM images (Fig. 7A) revealed a spiderweb-like structure with fiber diameters ranging from 20 to 200 nm, while high-magnification TEM images (Fig. 7B) highlighted the presence of interconnected nanoparticles (3–10 nm), forming a porous architecture. These results demonstrate the successful formation of stable Co_3O_4 nanofibers with a consistent morphology.

3.2. Gas sensing performance

The gas-sensing properties of the Co_3O_4 nanofibers were evaluated for ethanol (C_2H_5OH) detection across a range of concentrations (25–500 ppm) and operating temperatures (250–450 °C). The dynamic resistance of the sensor during cyclic ethanol exposures is shown in Fig. 8A. After ethanol injection, the sensor resistance increased rapidly, reflecting the reducing nature of ethanol. The base resistance in air gradually decreased with increasing temperature, as expected.

The relationship between sensor response gas and ethanol concentration at different temperatures is presented in Fig. 8B. The sensor response increased with ethanol concentration,

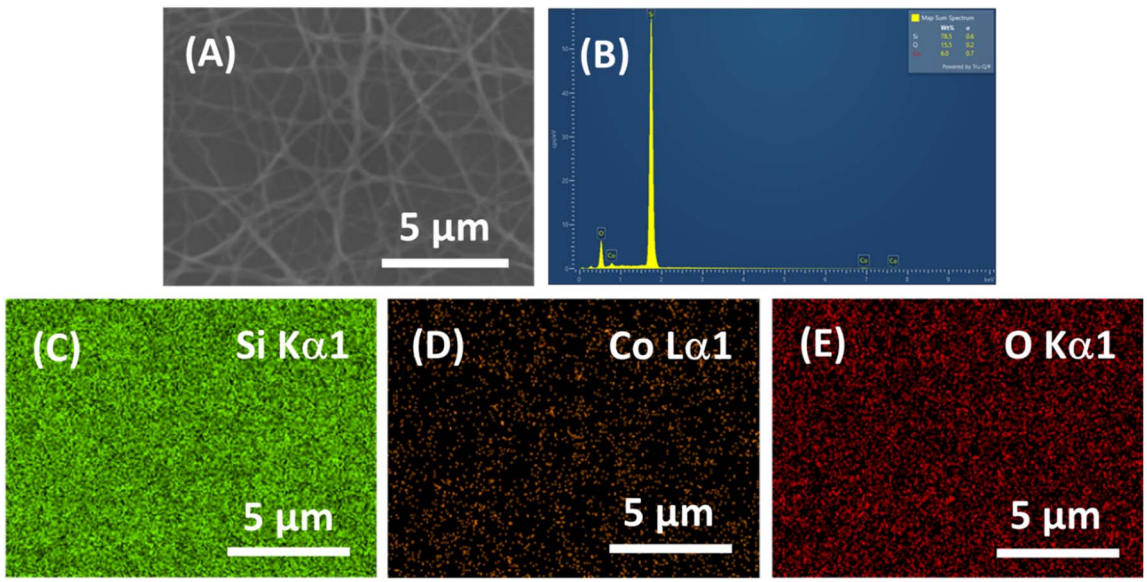

Fig. 5 (A) SEM image, (B) EDS spectrum and (C–E) EDS mapping of Co_3O_4 nanofibers.

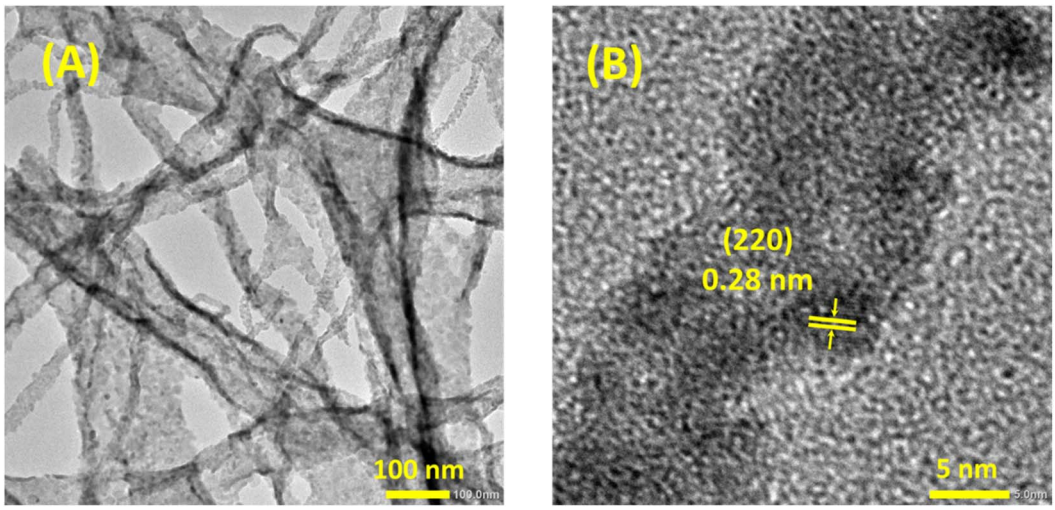

Fig. 7 TEM micrographs featuring the microstructure of annealed In_2O_3 polycrystalline nanofibers at varying levels of magnification: (A) lower magnification view and (B) higher magnification view.

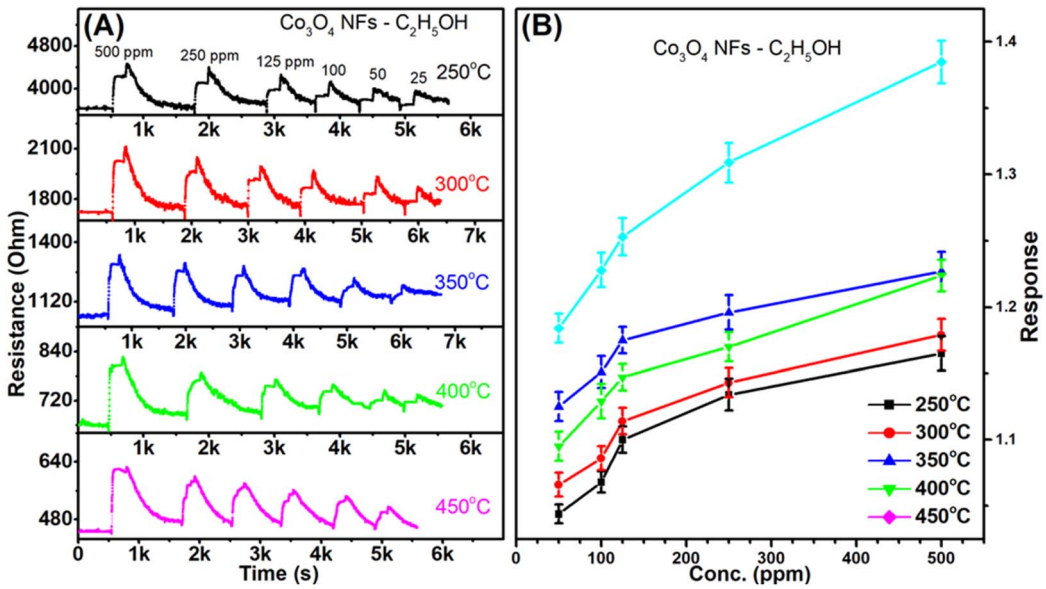

Fig. 8 Ethanol sensing performance of Co_3O_4 sensors: (A) dynamic resistance to ethanol concentrations ranging 50–500 ppm at various operating temperatures (250–450 °C); (B) sensor response as a function of ethanol concentration (50–500 ppm) at different working temperatures (250–450 °C).

exhibiting a rapid rise at lower concentrations (up to 125 ppm) before transitioning to a more linear trend, likely due to surface saturation effects. The optimal operating temperature was identified as 450 °C, at which the sensor achieved responses of 1.12, 1.18, 1.23, 1.25, 1.31 and 1.39 for concentrations of 25, 50, 100, 125, 250, and 500 ppm, respectively.

3.3. Gas sensing mechanism

Co_3O_4, a p-type semiconductor, operates *via* hole-dominated conduction. Upon exposure to ambient air, oxygen molecules adsorb onto the nanofiber surface, forming O^- and O^{2-} ions by sequestering electrons from the material. This increases the hole concentration and enhances conductivity.

When ethanol is introduced, it reacts with the adsorbed oxygen species, releasing trapped electrons back into the material where they recombine with holes. This reduces holes concentration, thereby increasing resistance.

The presence of oxygen defects in Co_3O_4 nanofibers plays a pivotal role in enhancing their gas-sensing capabilities, particularly for ethanol detection. Oxygen defects act as active sites for gas adsorption, significantly influencing the sensor's surface chemistry. When ethanol molecules interact with the sensor's surface, oxygen defects facilitate the adsorption and subsequent catalytic oxidation of ethanol. This reaction leads to a change in surface resistance, which is the primary sensing mechanism for Co_3O_4-based gas sensors. Specifically, the

Table 1 Comparison of ethanol sensing performance of Co_3O_4 nanomaterials in recent literature

Material	Method	T (°C)	C_2H_5OH conc. (ppm)	Response	Ref. (year)
Co_3O_4–Pt nanorods	Hydrothermal	250	100	1.35	23 (2023)
Co_3O_4 nanodisks	Hydrothermal	175	100	94%	26 (2023)
Au@Co_3O_4 core–shell nanoparticles	Wet chemical	250	2	1.7	27 (2022)
Co_3O_4–$MoTe_2$ nanocomposite	Wet chemical	25	1	10%	28 (2022)
Co_3O_4nanofibers	**Electrospinning**	**450**	**500**	**1.39**	**This work**

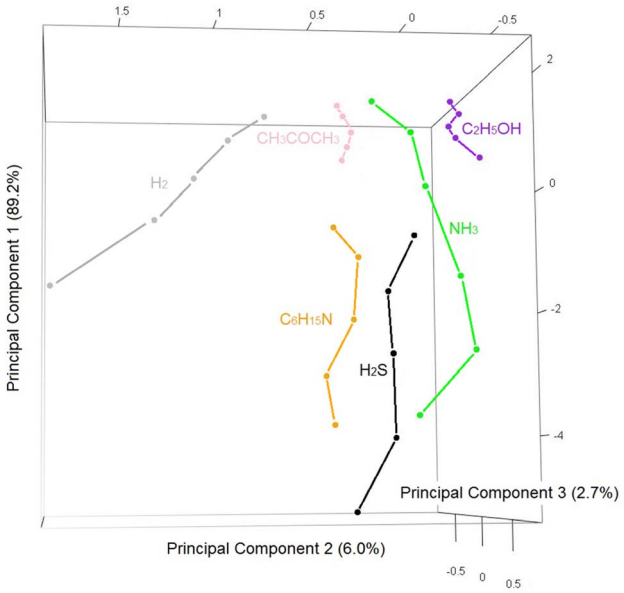

Fig. 9 Three-dimensional PCA plot of the sensor response values.

oxygen vacancies enhance the material's ability to chemisorb oxygen molecules from the air, which are then ionized into reactive oxygen species such as O^- or O_2^-.[24,25] These species participate in the redox reactions with ethanol, releasing electrons back into the conduction band, thereby modulating the sensor's electrical resistance.

Moreover, oxygen defects also impact the electron–hole recombination process. By trapping free electrons, oxygen vacancies prolong the lifetime of photogenerated charge carriers, which is critical for maintaining a high level of sensitivity. This mechanism ensures a more pronounced and stable change in resistance upon ethanol exposure, improving the signal-to-noise ratio and the overall performance of the sensor. Furthermore, the enhanced charge carrier dynamics associated with oxygen vacancies contribute to a lower operating temperature, reducing energy consumption and making the sensor more efficient.

To benchmark the performance of the Co_3O_4 nanofibers sensor, a comparative analysis with recent studies was conducted (Table 1). The results indicate that the Co_3O_4 nanofibers synthesized *via* electrospinning exhibit good ethanol sensing, achieving a response of 1.39 at 500 ppm and 450 °C. This compares favorably to other Co_3O_4-based sensors produced using methods such as hydrothermal synthesis and wet chemical routes.[23,26]

3.4. Thermal gas electronic nose

Although the Co_3O_4 nanofiber-based sensor has a high response towards ethanol compared to other tested gases, selectivity remains one of the limitations of metal oxide-based resistive sensors.[29] To address this, such sensors are often integrated into electronic nose systems, which typically rely on arrays of sensors based on different materials. However, this approach complicates miniaturization due to the varying requirements of the materials. An innovative alternative is to use a single material at different working temperatures.[30] In this study, response values obtained from the Co_3O_4 nanofiber sensor at the five different operating temperatures were combined and analyzed using multivariate statistical techniques.

Fig. 9 shows a principal component analysis (PCA) plot, showing the first three principal components that together account for 99.7% of the total variance. Despite the dimensional reduction, the data points corresponding to different gases are well-separated, indicating effective discrimination. Moreover, points for each gas lie along distinct lines rather than clusters, with points at the top of the graph representing low concentrations and points further down indicating higher concentrations.

The classification of the gases was carried out using linear discriminant analysis (LDA), with the results summarized in Table 2.

The analysis achieved perfect classification, with no misclassifications across 30 measurements, yielding an accuracy of 100.0%.

Once individual gases were identified, their concentrations were estimated using six different support vector regressors (SVRs), one for each gas. The regression results are shown in

Table 2 Gas classification by linear discriminant analysis. True gas on columns, predicted on rows

Pred./True	C_2H_5OH	$C_6H_{15}N$	CH_3COCH_3	H_2	H_2S	NH_3
C_2H_5OH	5					
$C_6H_{15}N$		5				
CH_3COCH_3			5			
H_2				5		
H_2S					5	
NH_3						5

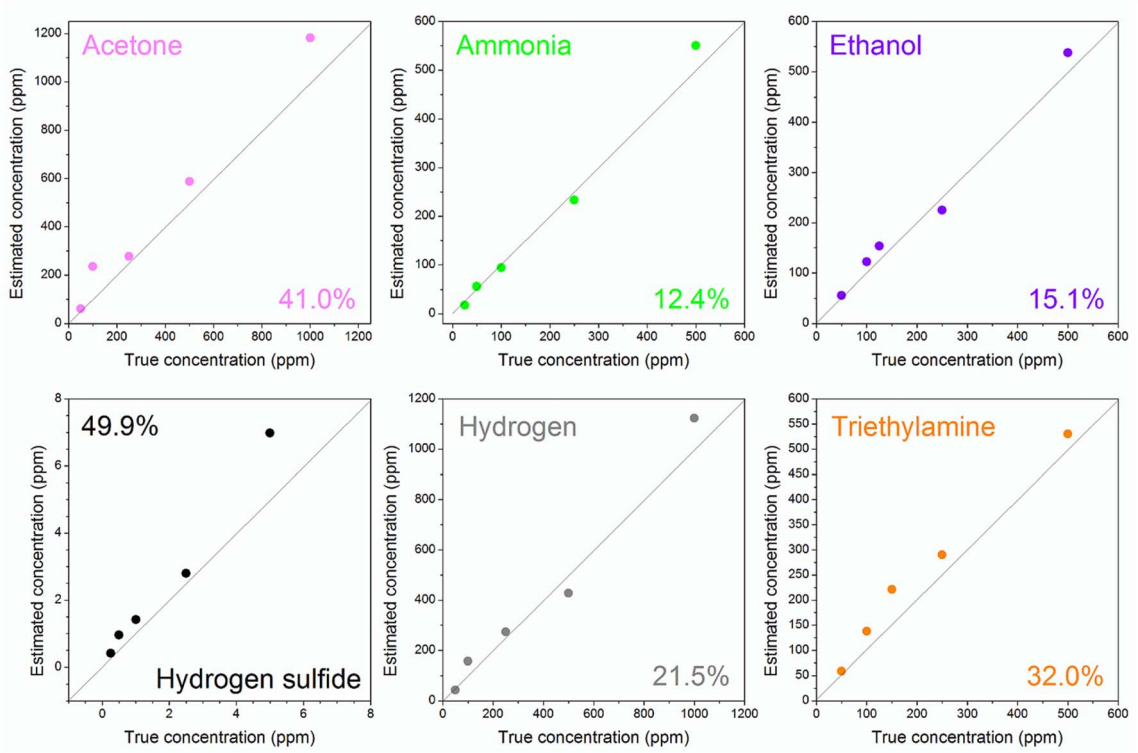

Fig. 10 Estimate of the gas concentration as a function of the true gas concentration for the tested gases.

Fig. 10, which compares estimated gas concentrations against true concentrations.

The data points lie close to the diagonal, indicating strong quantification performance. The error on the concentration estimate varies from gas to gas, and is reported in the boxes of Fig. 10. The electronic nose works relatively well for acetone, hydrogen sulfide and triethylamine, since it must be considered that the gas concentration spans many orders of magnitude (if the electronic nose estimates 2 ppm, there is the certainty that the true concentration is between 1 and 4 ppm, and not ppb). With hydrogen, ethanol and ammonia the electronic nose works very well, with an error ranging from 21.5 to 12.4%. The ability to accurately distinguish different gases and estimate their concentration is beyond the normal performance of a chemoresistive gas sensor, and is only possible with the thermal electronic nose approach.

4. Conclusions

This study demonstrates the successful synthesis of polycrystalline Co_3O_4 nanofibers through a two-step process involving electrospinning and thermal annealing. The resulting nanofibers show porous structures composed of interconnected nanoparticles with diameters ranging from 3 to 10 nm. The Co_3O_4 nanofibers were evaluated as resistive sensors for ethanol detection. The sensor achieved a notable response of 1.39 when exposed to 500 ppm of ethanol at an optimal working temperature of 450 °C. Thanks to the thermal electronic nose approach and the use of algorithms such as LDA and SVM, the sensor achieves performances unmatched by a simple chemical gas sensor: perfect classification (100% accuracy) for all tested gases and good concentration estimation, with an average error of 28.6%. Particularly strong performance was observed for ethanol and ammonia, with errors of 15.5 and 12.4%, respectively. These results demonstrate that electrospun polycrystalline Co_3O_4 nanofibers are promising candidates for the development of high-performance ethanol sensors and compact electronic noses, offering reliable classification and quantification capabilities across a wide range of gases. In addition to reducing the working temperature to lower power consumption, improving gas response—especially for breath diagnostics (challenging due to bio-interferents)—is essential for enhancing road safety.

Data availability

All data supporting the findings of this study are included in the manuscript. No additional data are available.

Conflicts of interest

The authors declare that they have no known competing financial interests or personal relationships that could have appeared to influence the work reported in this paper.

Acknowledgements

This work was financially supported by the Ministry of Science and Technology, under grant no. ĐTĐL.CN-35/23; the Air Force Office of Scientific under award number FA2386-22-1-4043.

References

1 S. Yang, H. Yin, Z. Wang, G. Lei, H. Xu, Z. Lan and H. Gu, Gas sensing performance of In_2O_3 nanostructures: a mini review, *Front. Chem.*, 2023, **11**, 1–7, DOI: 10.3389/fchem.2023.1174207.

2 C. Dong, R. Zhao, L. Yao, Y. Ran, X. Zhang and Y. Wang, A review on WO_3 based gas sensors: morphology control and enhanced sensing properties, *J. Alloys Compd.*, 2020, **820**, 153194, DOI: 10.1016/j.jallcom.2019.153194.

3 S. Li, C. Wang, Z. Lei, S. Sun, J. Gao, P. Cheng and H. Wang, Synergistic adsorption effect on Co_3O_4(1 1 0) surface to promote the ethanol sensing properties: experiment and theory, *Appl. Surf. Sci.*, 2023, **612**, 155776, DOI: 10.1016/j.apsusc.2022.155776.

4 F. Sun, Q. Li, Y. Bai, G. Zhang, S. Zheng, M. Peng, X. Chen, N. Lin and H. Pang, A controllable preparation of two-dimensional cobalt oxalate-based nanostructured sheets for electrochemical energy storage, *Chin. Chem. Lett.*, 2022, **33**, 3249–3254, DOI: 10.1016/j.cclet.2021.10.075.

5 L. N. Jin, J. G. Wang, X. Y. Qian, D. Xia and M. D. Dong, Catalytic Activity of Co_3O_4 Nanomaterials with Different Morphologies for the Thermal Decomposition of Ammonium Perchlorate, *J. Nanomater.*, 2015, **2015**, 854310, DOI: 10.1155/2015/854310.

6 C. Hu, L. Yu, S. Li, M. Yin, H. Du and H. Li, Sacrificial template triggered to synthesize hollow nanosheet-assembled Co_3O_4 microtubes for fast triethylamine detection, *Sens. Actuators, B*, 2022, **355**, 131246, DOI: 10.1016/j.snb.2021.131246.

7 Y. Tan, Q. Gao, C. Yang, K. Yang, W. Tian and L. Zhu, One-dimensional porous nanofibers of Co_3O_4 on the carbon matrix from human hair with superior lithium ion storage performance, *Sci. Rep.*, 2015, **5**, 15–17, DOI: 10.1038/srep12382.

8 J. M. Xu and J. P. Cheng, The advances of Co_3O_4 as gas sensing materials: a review, *J. Alloys Compd.*, 2016, **686**, 753–768, DOI: 10.1016/j.jallcom.2016.06.086.

9 L. Li, Q. Diao, Z. Liu, G. Zhu, C. Huang, G. Shi, X. Huang, J. Zhang and M. Jiao, Facile synthesis of oxygen vacancies mediated Co_3O_4 by Mn doping for high-performance ethanol sensing, *Vacuum*, 2024, **224**, 113202, DOI: 10.1016/j.vacuum.2024.113202.

10 W. Wang, J. Xian, J. Li, M. Yu, Q. Duan, C. M. Leung, M. Zeng and X. Gao, Construction of Co_3O_4/SnO_2 yolk-shell nanofibers for acetone gas detection, *Sens. Actuators, B*, 2024, **398**, 134724, DOI: 10.1016/j.snb.2023.134724.

11 J. Zhang, D. Leng, G. Li, J. Liu, H. Wang, Y. Zhu, H. Lu, J. Gao and B. Zhu, Bimetallic–organic framework-derived Co_3O_4–ZnO heterojunction nanofibers: a new kind of emerging porous nanomaterial for enhanced ethanol sensing, *Sens. Actuators, B*, 2021, **349**, 130732, DOI: 10.1016/j.snb.2021.130732.

12 P. Karnati, S. Akbar and P. A. Morris, Conduction mechanisms in one dimensional core–shell nanostructures for gas sensing: a review, *Sens. Actuators, B*, 2019, **295**, 127–143, DOI: 10.1016/j.snb.2019.05.049.

13 https://www.osha.gov/chemicaldata/1034.

14 Y. Zhang, Z. Duan, H. Zou and M. Ma, Fabrication of electrospun $LaFeO_3$ nanotubes *via* annealing technique for fast ethanol detection, *Mater. Lett.*, 2018, **215**, 58–61, DOI: 10.1016/j.matlet.2017.12.062.

15 I. Cho, J. Ko, D. D. O. Henriquez, D. Yang and I. Park, Recent Advances in 1D Nanostructure Assembly and Direct Integration Methods for Device Applications, *Small Methods*, 2024, 2400474, DOI: 10.1002/smtd.202400474.

16 D. Han, Y. Ji, F. Gu and Z. Wang, Cobalt oxide nanorods with special pore structure for enhanced ethanol sensing performance, *J. Colloid Interface Sci.*, 2018, **531**, 320–330, DOI: 10.1016/j.jcis.2018.07.064.

17 N. H. Tan, D. Thi Thanh Le, T. T. Hoang, N. M. Duy, M. Tonezzer, C. Thi Xuan, N. Van Duy and N. D. Hoa, Metal-decorated indium oxide nanofibers used as nanosensor for triethylamine sensing towards seafood quality monitoring, *Colloids Surf., A*, 2024, **703**, 135268, DOI: 10.1016/j.colsurfa.2024.135268.

18 Y. Zhang, J. Li, Q. Li, L. Zhu, X. Liu, X. Zhong, J. Meng and X. Cao, Preparation of In_2O_3 ceramic nanofibers by electrospinning and their optical properties, *Scr. Mater.*, 2007, **56**, 409–412, DOI: 10.1016/j.scriptamat.2006.10.032.

19 F. Mou, J. Guan, W. Shi, Z. Sun and S. Wang, Oriented Contraction: A Facile Nonequilibrium Heat-Treatment Approach for Fabrication of Maghemite Fiber-in-Tube and Tube-in-Tube Nanostructures, *Langmuir*, 2010, **26**, 15580–15585, DOI: 10.1021/la102830p.

20 A. A. Muleja and B. B. Mamba, Development of calcined catalytic membrane for potential photodegradation of Congo red in aqueous solution, *J. Environ. Chem. Eng.*, 2018, **6**, 4850–4863, DOI: 10.1016/j.jece.2018.07.004.

21 E. A. Van Etten, E. S. Ximenes, L. T. Tarasconi, I. T. S. Garcia, M. M. C. Forte and H. Boudinov, Insulating characteristics of polyvinyl alcohol for integrated electronics, *Thin Solid Films*, 2014, **568**, 111–116, DOI: 10.1016/j.tsf.2014.07.051.

22 F. Mou, J. Guan, W. Shi, Z. Sun and S. Wang, Oriented Contraction: A Facile Nonequilibrium Heat-Treatment Approach for Fabrication of Maghemite Fiber-in-Tube and Tube-in-Tube Nanostructures, *Langmuir*, 2010, **26**, 15580–15585, DOI: 10.1021/la102830p.

23 T. T. Le Dang, T. N. T. Do, V. M. Do, M. Tonezzer, V. D. N. Tran, T. X. Chu, M. H. Chu, V. D. Nguyen and D. H. Nguyen, Eco-friendly facile synthesis of Co_3O_4–Pt nanorods for ethylene detection towards fruit quality monitoring, *Sens. Actuators, A*, 2023, **362**, 114607, DOI: 10.1016/j.sna.2023.114607.

24 M. Al-Hashem, S. Akbar and P. Morris, Role of Oxygen Vacancies in Nanostructured Metal-Oxide Gas Sensors: A Review, *Sens. Actuators, B*, 2019, **301**, 126845, DOI: 10.1016/j.snb.2019.126845.

25 S.-S. Li, Q.-Q. Xu, J.-T. Xu, G. Yan, Y.-X. Zhang, S.-W. Li and L.-C. Yin, Engineering Co^{2+}/Co^{3+} redox activity of Ni-mediated porous Co_3O_4 nanosheets for superior Hg(II) electrochemical sensing: insight into the effect of valence

change cycle and oxygen vacancy on electroanalysis, *Sens. Actuators, B*, 2022, **354**, 131095, DOI: **10.1016/j.snb.2021.131095**.

26 K. D. Bhalerao, M. Khan, Y. T. Nakate, R. M. Kadam, S. Manzoor, S. Masrat, P. Mishra, U. T. Nakate and R. Ahmad, Co_3O_4 hexagonal nanodisks: synthesis and efficient ethanol gas sensing application, *Surf. Interfaces*, 2023, **42**, 103350, DOI: **10.1016/j.surfin.2023.103350**.

27 H. Y. Lee, J. H. Bang, S. M. Majhi, A. Mirzaei, K. Y. Shin, D. J. Yu, W. Oum, S. Kang, M. L. Lee, S. S. Kim and H. W. Kim, Conductometric ppb-level acetone gas sensor based on one-pot synthesized Au@Co_3O_4 core–shell nanoparticles, *Sens. Actuators, B*, 2022, **359**, 131550, DOI: **10.1016/j.snb.2022.131550**.

28 F. Chen, Y. Zhang, D. Wang, T. Wang, J. Zhang and D. Zhang, High performance ammonia gas sensor based on electrospinned Co_3O_4 nanofibers decorated with hydrothermally synthesized $MoTe_2$ nanoparticles, *J. Alloys Compd.*, 2022, **923**, 166355, DOI: **10.1016/j.jallcom.2022.166355**.

29 M. Tonezzer, D. Thi Thanh Le, L. Van Duy, N. D. Hoa, F. Gasperi, N. Van Duy and F. Biasioli, Electronic noses based on metal oxide nanowires: a review, *Nanotechnol. Rev.*, 2022, **11**, 897–925, DOI: **10.1515/ntrev-2022-0056**.

30 N. X. Thai, N. Van Duy, C. M. Hung, H. Nguyen, M. Tonezzer, N. Van Hieu and N. D. Hoa, Prototype edge-grown nanowire sensor array for the real-time monitoring and classification of multiple gases, *J. Sci.: Adv. Mater. Devices*, 2020, **5**, 409–416, DOI: **10.1016/j.jsamd.2020.05.005**.